Journal of Physics: Conference Series **2494** (2023) 012017 doi:10.1088/1742-6596/2494/1/012017

Optimal Phase Sensitivity in an Unbalanced Mach-Zehnder Interferometer

Stefan Ataman

Extreme Light Infrastructure - Nuclear Physics (ELI-NP),
"Horia Hulubei" National R&D Institute for Physics and Nuclear Engineering (IFIN-HH),
30 Reactorului Street, 077125 Bucharest-Măgurele, Romania

E-mail: stefan.ataman@eli-np.ro

Abstract. In this work we address the problem of phase sensitivity optimization for an unbalanced Mach-Zehnder interferometer. While the quantum Fisher information can be employed in order to obtain the optimum transmission coefficient for the first beam splitter, this is no longer true for the second one, whose optimization is detection-scheme dependent. We thus consider three commonly used detection schemes and provide the optimal solution for each case. We also provide applications of the optimization method showing that for some input states a non-balanced Mach-Zehnder interferometer can outperform its balanced counterpart in terms of phase sensitivity.

1. Introduction

Optical interferometry is a mature technology that saw a renaissance in the last decade with diverse applications such as gravitational wave detection [1, 2, 3], quantum enhanced metrology [4, 5, 6], quantum-enhanced dark matter searches [7] or biological quantum imaging [8, 9].

Of great help in both the performance assessment and the optimization of an interferometer is the theoretical best limit for a parameter estimation known as the quantum Cramér-Rao bound (QCRB) [10, 11, 12]. For the derivation of this bound one needs the quantum Fisher information (QFI) [12, 13]. For example, applying a classical input state at the input of an interferometer implies a shot-noise limit (SNL) for the phase sensitivity, while the more favourable Heisenberg limit (HL) requires non-classical input states [4, 5, 13].

When assessing the phase sensitivity of an interferometer, most authors assume it balanced [14, 15, 16, 17, 18, 19]. This is no accident since this choice proves to be optimal for many input states and for detection schemes not having access to an external phase reference [16, 17, 18, 20, 21]. However, when considering a detection scheme having access to an external reference, this assertion is not always true [22, 23] and, following reference [21], the relevant QCRB in this case is obtained by employing the single-parameter QFI. In order to reach this limit, though, an unbalanced interferometer is needed [22].

When unbalancing a Mach-Zehnder interferometer (MZI), the problem of finding the transmission coefficients of the two beam splitters (BS) composing the MZI that optimize the phase sensitivity arises [23, 22, 24, 25]. We address this problem in this work. We assume a pure input state and a lossless system. As we will outline, the optimum transmission coefficient of the first BS (T) can be unambiguosly determined with the help of QFI [23]. Indeed, one can

take advantage of the fact that the QFI is insensitive in respect with the presence or absence of the second BS [23, 26].

The optimization of the second BS's transmission coefficient (T') turns out to be detection scheme dependent, however a general framework for determining it can be outlined [25]. While many detection schemes have been discussed in the literature [27, 28, 29, 30, 31, 32, 33, 34], we consider in this work only three among them, namely: the difference-intensity detection [20, 25, 28] the single-mode intensity detection [20, 25, 28] and balanced homodyne detection (BHD) [22, 25, 27, 28] schemes.

This paper is structured as follows. In Section 2 the quantum optical description of our system is provided. In Section 3 we discuss the QFI-based optimization of the first BS' transmission coefficient. The detection scheme-dependent optimization of the second BS's transmission coefficient is discussed at length in Section 4. Some phase sensitivity optimizations for an unbalanced MZI are given in Section 5 and finally, the conclusions are drawn in Section 6.

2. Quantum optical description of an unbalanced Mach-Zehnder interferometer

We consider the MZI depicted in Fig. 1. The input state (denoted $|\psi_{in}\rangle$) is assumed to be pure and all optical elements are assumed lossless. The MZI is parametrized via the two beam splitters' transmission coefficients T (for BS_1), respectively, T' (for BS_2). The internal phase shift (denoted φ) is assumed in the lower arm of the interferometer. The beam splitters obey the usual constraints $|T|^2+|R|^2=1$ and $T^*R+TR^*=0$ [35]. Here R denotes the reflection coefficient of the first beam splitter (BS_1). It will prove advantageous to use the parametrization

$$\begin{cases} T=\cos\frac{\vartheta}{2} \\ R=i\sin\frac{\vartheta}{2}. \end{cases} \tag{1}$$

Similarly, for BS_2 we have $T'=\cos\frac{\vartheta'}{2}$ and $R'=i\sin\frac{\vartheta'}{2}$. The introduced pseudo-angles obey $\{\vartheta,\vartheta'\}\in[0,\pi]$. We will employ the input Schwinger pseudo-angular momentum operators $\hat{J}_x=(\hat{a}_0^\dagger\hat{a}_1+\hat{a}_0\hat{a}_1^\dagger)/2$, $\hat{J}_y=(\hat{a}_0^\dagger\hat{a}_1-\hat{a}_0\hat{a}_1^\dagger)/2i$ and $\hat{J}_z=(\hat{a}_0^\dagger\hat{a}_0-\hat{a}_1^\dagger\hat{a}_1)/2$ [36, 37], where $\hat{a}_l$ ($\hat{a}_l^\dagger$) denotes the usual annihilation (creation) operators for the input mode $l\in\{0,1\}$ [35]. The input total photon number operator is $\hat{N}=\hat{n}_0+\hat{n}_1$, where $\hat{n}_l=\hat{a}_l^\dagger\hat{a}_l$ denotes the number operator for a mode l. Throughout this work, given a quantum state $|\psi\rangle$, the average of an operator is given by $\langle\hat{O}\rangle=\langle\psi|\hat{O}|\psi\rangle$ while its variance is $\Delta^2\hat{O}=\langle\psi|\hat{O}^2|\psi\rangle-\langle\hat{O}\rangle^2$. The covariance of two operators $\hat{O}_1$ and $\hat{O}_2$ is defined by $\mathrm{Cov}\left(\hat{O}_1,\hat{O}_2\right)=\langle\hat{O}_1\hat{O}_2\rangle-\langle\hat{O}_1\rangle\langle\hat{O}_2\rangle$ and the symmetrized covariance of two non-commuting operators is

$$\widehat{\mathrm{Cov}}\left(\hat{O}_1,\hat{O}_2\right)=\frac{\langle\hat{O}_1\hat{O}_2\rangle+\langle\hat{O}_2\hat{O}_1\rangle}{2}-\langle\hat{O}_1\rangle\langle\hat{O}_2\rangle. \tag{2}$$

Returning to the MZI from Fig. 1, the output state can be formally written as

$$|\psi_{out}\rangle=\hat{U}_{BS}\left(\vartheta'\right)\hat{U}_\varphi\hat{U}_{BS}\left(\vartheta\right)|\psi_{in}\rangle \tag{3}$$

and we model each beam splitter via the unitary operator $\hat{U}_{BS}\left(\varpi\right)=e^{i\varpi\hat{J}_x}$ where $\varpi\in\{\vartheta,\vartheta'\}$. The effect of the phase shift is modeled via $\hat{U}_\varphi$ and we will detail this operator in the next section.

For future convenience we introduce the coefficients

$$\begin{cases} \mathcal{A}_{40}=\cos\frac{\vartheta}{2}\cos\frac{\vartheta'}{2}-\sin\frac{\vartheta}{2}\sin\frac{\vartheta'}{2}e^{-i\varphi} \\ \mathcal{A}_{41}=i\left(\cos\frac{\vartheta}{2}\sin\frac{\vartheta'}{2}e^{-i\varphi}+\sin\frac{\vartheta}{2}\cos\frac{\vartheta'}{2}\right) \\ \mathcal{A}_{50}=i\left(\cos\frac{\vartheta}{2}\sin\frac{\vartheta'}{2}+\sin\frac{\vartheta}{2}\cos\frac{\vartheta'}{2}e^{-i\varphi}\right) \\ \mathcal{A}_{51}=\cos\frac{\vartheta}{2}\cos\frac{\vartheta'}{2}e^{-i\varphi}-\sin\frac{\vartheta}{2}\sin\frac{\vartheta'}{2}. \end{cases} \tag{4}$$

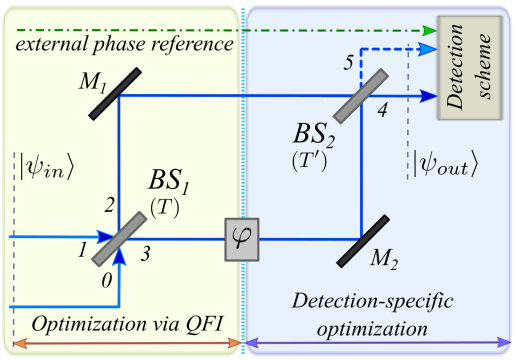

Figure 1. The unbalanced Mach-Zehnder under consideration. The optimization will be a two-step process, as outlined in the main text.

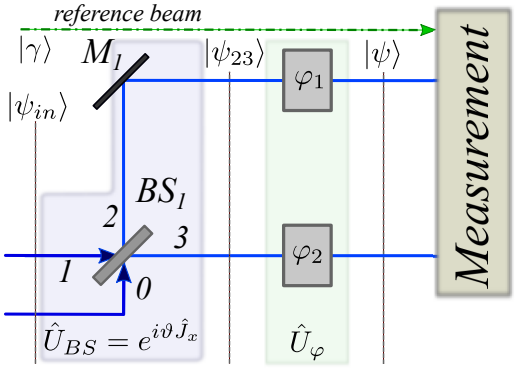

Figure 2. The optimization of the first beam splitter's transmission coefficient ($T = \cos\vartheta/2$) is performed via the appropriate QFI.

and

$$\begin{cases} K_x = 2\mathrm{Re}\{\mathcal{A}_{40}\mathcal{A}_{41}^*\} = \sin\vartheta'\sin\varphi \\ K_y = 2\mathrm{Im}\{\mathcal{A}_{40}\mathcal{A}_{41}^*\} = -\left(\sin\vartheta\cos\vartheta' + \cos\vartheta\sin\vartheta'\cos\varphi\right) \\ K_z = 2|\mathcal{A}_{40}|^2 - 1 = \cos\vartheta\cos\vartheta' - \sin\vartheta\sin\vartheta'\cos\varphi \end{cases} \tag{5}$$

and it is easy to see that the above terms obey the constraint $K_x^2 + K_y^2 + K_z^2 = 1$ [23].

3. QFI-based optimization of first BS's transmission coefficient

As depicted in Fig. 1, the phase sensitivity optimization problem is split into two smaller ones. The first one deals with finding the transmission coefficient (1) of BS_1 (denoted T_{opt}) that maximizes the QFI. While we can use the MZI output state (3) for our calculations, is more convenient to stop after the internal phase shift, thus arriving at the scenario depicted in Fig. 2. As previously mentioned, this is possible because BS_2 has no inffluence whatsoever in the QFI calculations [23, 26]. The wavevector we will thus consider for all QFI evaluations will be

$$|\psi\rangle = \hat{U}_\varphi |\psi_{23}\rangle = \hat{U}_\varphi \hat{U}_{BS}(\vartheta) |\psi_{in}\rangle . \tag{6}$$

3.1. The scenario when an external phase reference is unavailable

If one assumes that an external phase reference is unavailable, the extra resources that the QFI automatically takes into consideration must be discarded. One solution implies averaging out the input state in respect with a common phase [21]. This however transforms the input state from a pure one to a density matrix and all the simplicity in the evaluation of the QFI is lost. We thus opt for the second technique, namely we introduce a second phase shift (see Fig. 2) and evaluate the two-parameter QFI [18, 21, 22]. We thus consider two phase shifts in our MZI, φ_1 (φ_2) in the upper (lower) arm of the interferometer. If will prove more convenient to make a variable change and consider the phase sum/difference *i. e.* $\varphi_s = \varphi_1 + \varphi_2$ and $\varphi_d = \varphi_1 - \varphi_2$. The effect of these phase shifts is modelled via the unitary operator

$$\hat{U}_\varphi = e^{-\varphi_1\hat{n}_2}e^{-i\varphi_2\hat{n}_3} = e^{-\varphi_s\frac{\hat{N}}{2}}e^{-i\varphi_d\hat{J}_z}. = e^{-\varphi_s\hat{G}_s}e^{-i\varphi_d\hat{G}_d} \tag{7}$$

where the generators are $\hat{G}_d = \hat{J}_z = (\hat{n}_2 - \hat{n}_3)/2$ and $\hat{G}_s = \hat{N}/2 = (\hat{n}_2 + \hat{n}_3)/2$ [13]. Equation (6) can now be expressed in respect with the sum/difference phase shifts, therefore

$$|\psi\rangle = e^{-i\hat{G}_d\varphi_d}e^{-i\hat{G}_s\varphi_s}|\psi_{23}\rangle. \tag{8}$$

We introduce the Fisher matrix elements $\mathcal{F}_{ss} = 4\Delta^2\hat{G}_s$, $\mathcal{F}_{dd} = 4\Delta^2\hat{G}_d$ and $\mathcal{F}_{sd} = 4\mathrm{Cov}(\hat{G}_s, \hat{G}_d)$. Expressing them in respect with the input field operators yields [23]

$$\begin{cases} \mathcal{F}_{ss} = \Delta^2\hat{N} \\ \mathcal{F}_{dd} = 4\left(\sin^2\vartheta\Delta^2\hat{J}_y + \cos^2\vartheta\Delta^2\hat{J}_z - \sin 2\vartheta\widehat{\mathrm{Cov}}\left(\hat{J}_y, \hat{J}_z\right)\right) \\ \mathcal{F}_{sd} = -2\sin\vartheta\mathrm{Cov}\left(\hat{J}_y, \hat{N}\right) + 2\cos\vartheta\mathrm{Cov}\left(\hat{J}_z, \hat{N}\right). \end{cases} \tag{9}$$

Since we are interested in a difference-difference phase sensitivity [18, 21] (see also Appendix E in [23]) we introduce the two-parameter QFI $\mathcal{F}^{(2p)} = \mathcal{F}_{dd} - \mathcal{F}_{sd}^2/\mathcal{F}_{ss}$ and this QFI implies the difference-difference QCRB,

$$\Delta\varphi_{QCRB}^{(2p)} = \frac{1}{\sqrt{\mathcal{F}^{(2p)}}}. \tag{10}$$

This is the "true" interferometric phase sensitivity for a MZI with a detection scheme not having access to an external phase reference [21, 22, 23]. We now wish to find T_{opt} that maximizes $\mathcal{F}^{(2p)}$. Following reference [23], we can rewrite the two-parameter QFI as

$$\mathcal{F}^{(2p)} = C_0 + C_1|TR|^2 + C_2|TR|\left(|T|^2 - |R|^2\right) \tag{11}$$

where the C-coefficients are given in Appendix A. One can thus find a closed-form solution to the transmission coefficient T_{opt} that will maximise the two-parameter QFI to $\mathcal{F}_{max}^{(2p)}$ (see [23], Section VA). We describe below the possible scenarios that arise during this optimization:
A) The case $C_1 = C_2 = 0$ implies $\mathcal{F}^{(2p)} = C_0$, hence and the value of T becomes irrelevant.
B) The case $C_1 \neq 0$, $C_2 = 0$ implies two sub-cases: i) if $C_1 > 0$, then $\mathcal{F}^{(2p)}$ is maximized for BS_1 balanced ($T_{opt} = 1/\sqrt{2}$) and ii) if $C_1 < 0$, $\mathcal{F}^{(2p)}$ maximizes in the degenerate case ($T_{opt} = 0/1$).
C) In the most general case when $C_1 \neq 0$ and $C_2 \neq 0$, the optimum transmission coefficient is given in equation (32) from reference [23]. Plugging this value into equation (11) yields the maximum two-parameter QFI, $\mathcal{F}_{max}^{(2p)} = C_0 + C_1/8 + \sqrt{C_1^2 + 4C_2^2}/8$.

3.2. The scenario when an external phase reference is available
In this case we have the phase shift generator $\hat{G} = \hat{n}_3$, the (single-parameter) QFI can thus be expressed as $\mathcal{F}^{(i)} = 4\Delta^2\hat{G} = 4\Delta^2\hat{n}_3$ [13, 23], and this implies the single-parameter QCRB

$$\Delta\varphi_{QCRB}^{(i)} = \frac{1}{\sqrt{\mathcal{F}^{(i)}}}. \tag{12}$$

This optimum phase sensitivity corresponds to the case when an external phase reference is available [21, 22]. As discussed previously in the literature, one does not need to compute $\mathcal{F}^{(i)}$ separately since we can take advantage of the Fisher matrix elements previously computed *i. e.* $\mathcal{F}^{(i)} = \mathcal{F}_{ss} + \mathcal{F}_{dd} - 2\mathcal{F}_{sd}$ [22, 23]. We rewrite now the single-parameter QFI as

$$\mathcal{F}^{(i)} = C_0' + |TR|^2C_1' + |TR|(|T|^2 - |R|^2)C_2' + (|T|^2 - |R|^2)C_3' + |TR|C_4' \tag{13}$$

where the C'-coefficient are given in Appendix B. When maximizing $\mathcal{F}^{(i)}$ in respect with T we find the following situations:
A) If the input state obeys $\langle\hat{a}_0\rangle = 0$ this implies $C_2' = C_4' = 0$. We now have two sub-cases:
A1) If $C_3' = 0$, too, then: i) if $C_1' < 0$ then the optimum is in the degenerate case *i. e.* $T_{opt} = 0/1$ and $\mathcal{F}_{max}^{(i)} = C_0'$,
ii) if $C_1' > 0$ then the optimum is again in the balanced case, *i. e.* $T_{opt} = 1/\sqrt{2}$ and $\mathcal{F}_{max}^{(i)} = C_0' + C_1'/4$.

A2) For the general case with $\{C_1', C_3'\} \neq 0$, we have the scenarios: i) if the constraints

$$\begin{cases} \Delta^2 \hat{J}_y \geq \frac{\Delta^2 \hat{n}_1 - \mathrm{Cov}(\hat{n}_0, \hat{n}_1)}{2} \\ \Delta^2 \hat{J}_y \geq \frac{\Delta^2 \hat{n}_0 - \mathrm{Cov}(\hat{n}_0, \hat{n}_1)}{2} \end{cases} \tag{14}$$

are satisfied, then $T_{opt} = \sqrt{1/2 + C_3'/C_1'}$ implying $\mathcal{F}_{max}^{(i)} = C_0' + C_1' \left(1/4 + {C_3'}^2/{C_1'}^2\right)$
ii) if the conditions

$$\begin{cases} \Delta^2 \hat{J}_y \geq \frac{\Delta^2 \hat{n}_1 - \mathrm{Cov}(\hat{n}_0, \hat{n}_1)}{2} \\ \Delta^2 \hat{J}_y < \frac{\Delta^2 \hat{n}_0 - \mathrm{Cov}(\hat{n}_0, \hat{n}_1)}{2} \end{cases} \tag{15}$$

are met, then the optimal transmission coefficient is found in the degenerate case $T_{opt} = 0$ and $\mathcal{F}_{max}^{(i)} = C_0' - C_3' = 4\left(\Delta^2 \hat{n}_0 + \mathrm{Cov}(\hat{n}_0, \hat{n}_1)\right)$.
iii) if the conditions

$$\begin{cases} \Delta^2 \hat{J}_y < \frac{\Delta^2 \hat{n}_1 - \mathrm{Cov}(\hat{n}_0, \hat{n}_1)}{2} \\ \Delta^2 \hat{J}_y \geq \frac{\Delta^2 \hat{n}_0 - \mathrm{Cov}(\hat{n}_0, \hat{n}_1)}{2} \end{cases} \tag{16}$$

are satisfied, then the optimal transmission coefficient is again in the degenerate case $T_{opt} = 1$ and we have $\mathcal{F}_{max}^{(i)} = C_0' + C_3' = 4\left(\Delta^2 \hat{n}_1 + \mathrm{Cov}(\hat{n}_0, \hat{n}_1)\right)$.
iv) finally, if we have

$$\begin{cases} \Delta^2 \hat{J}_y < \frac{\Delta^2 \hat{n}_1 - \mathrm{Cov}(\hat{n}_0, \hat{n}_1)}{2} \\ \Delta^2 \hat{J}_y < \frac{\Delta^2 \hat{n}_0 - \mathrm{Cov}(\hat{n}_0, \hat{n}_1)}{2}, \end{cases} \tag{17}$$

the optimal transmission coefficient is in the degenerate case yielding $T_{opt} = 0$ for $C_3' < 0$ and $T_{opt} = 1$ for $C_3' > 0$.
B) The second scenario allowing a simple solution is found when $C_1' = C_2' = 0$. We get

$$T_{opt} = \sqrt{\frac{1}{2} + \frac{|C_3'|\mathrm{sgn}(C_3')}{\sqrt{4(C_3')^2 + (C_4')^2}}} \tag{18}$$

valid if $C_4' > 0$ and the maximum QFI is given by $\mathcal{F}_{max}^{(i)} = C_0' + \sqrt{4(C_3')^2 + (C_4')^2}/2$. For $C_4' < 0$ we have the optimum QFI in degenerate case with $T_{opt} = 0$ if $C_3' < 0$ and $T_{opt} = 1$ if $C_3' > 0$.
C) The optimum transmission coefficient when none of the previously mentioned simplifications apply is given in reference [23], equation (48).

4. Phase sensitivity optimization of an unbalanced MZI

From this point on, we assume that the first BS was already optimized via the QFI, as described in Section 3. We wish to optimize the MZI phase sensitivity and this involves optimization of a two-variable function [25]. Indeed, one finds through direct calculation that, regardless on the detection scheme employed, the phase sensitivity will depend on both the transmission coefficient of the second BS (ϑ') and the total internal phase shift (φ). We thus apply the usual extremization of a two variable function. A first set of the constraints

$$\begin{cases} \partial_{\vartheta'} \Delta\varphi(\vartheta', \varphi) = \frac{\partial \Delta\varphi(\vartheta', \varphi)}{\partial \vartheta'} = 0 \\ \partial_{\varphi} \Delta\varphi(\vartheta', \varphi) = \frac{\partial \Delta\varphi(\vartheta', \varphi)}{\partial \varphi} = 0. \end{cases} \tag{19}$$

yields a number of solutions, $(\vartheta'_{opt}, \varphi_{opt})$. Since, in the general case, the resulting pairs $(\vartheta'_{opt}, \varphi_{opt})$, are not necessarily extrema points, we must also impose a supplementary set of constraints, see reference [25], equation (38). In the following we apply this optimization to three often used detection schemes.

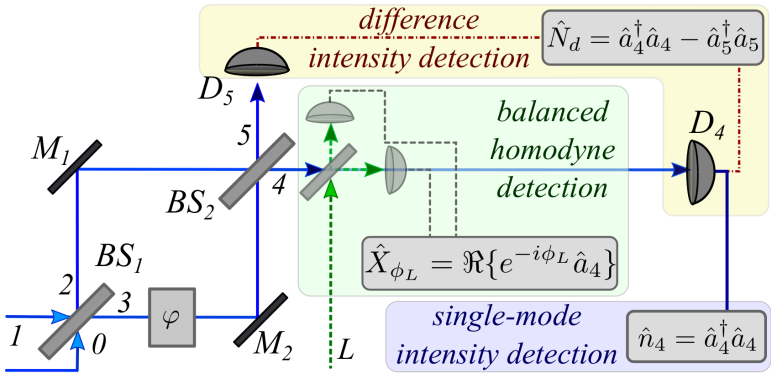

Figure 3. The three detection schemes considered in this work. See details in the main text.

4.1. Phase sensitivity optimization for a difference intensity detection scheme
In the difference-intensity detection scheme, we employ as observable the difference between the output photo-currents, $\hat{N}_d = \hat{n}_4 - \hat{n}_5$ (see Fig. 3). Expressing $\hat{N}_d$ in respect with the input field operators yields $\hat{N}_d = 2K_x\hat{J}_x + 2K_y\hat{J}_y + 2K_z\hat{J}_z$ [25]. The variance of the operator $\hat{N}_d$ is

$$\Delta^2\hat{N}_d = 4K_x^2\Delta^2\hat{J}_x + 4K_y^2\Delta^2\hat{J}_y + 4K_z^2\Delta^2\hat{J}_z + 8K_xK_z\widehat{\mathrm{Cov}}\left(\hat{J}_x,\hat{J}_z\right) + 8K_xK_y\widehat{\mathrm{Cov}}\left(\hat{J}_x,\hat{J}_y\right) + 8K_yK_z\widehat{\mathrm{Cov}}\left(\hat{J}_y,\hat{J}_z\right), \tag{20}$$

and phase sensitivity is given by

$$\Delta\varphi_{df} = \frac{\sqrt{\Delta^2\hat{N}_d}}{2\left|\langle\hat{J}_x\rangle\cos\varphi + \left(\cos\vartheta\,\langle\hat{J}_y\rangle + \sin\vartheta\langle\hat{J}_z\rangle\right)\sin\varphi\right||\sin\vartheta'|}. \tag{21}$$

This phase sensitivity can be optimized and a closed-form solution for both ϑ'_{opt} and φ_{opt} is possible, see reference [25], Appendix E.

4.2. Phase sensitivity optimization for a single mode detection scheme
In this scheme we employ a single photo-detector at output port 4, the observable conveying information being $\hat{n}_4$ (see Fig. 3). Expressing it in respect with the input field operator yields $\hat{n}_4 = \hat{N}/2 + K_x\hat{J}_x + K_y\hat{J}_y + K_z\hat{J}_z$. The variance is found to be [25],

$$\Delta^2\hat{n}_4 = \frac{1}{4}\Delta^2\hat{N} + K_x^2\Delta^2\hat{J}_x + K_y^2\Delta^2\hat{J}_y + K_z^2\Delta^2\hat{J}_z + 2K_xK_y\widehat{\mathrm{Cov}}\left(\hat{J}_x,\hat{J}_y\right) + 2K_xK_z\widehat{\mathrm{Cov}}\left(\hat{J}_x,\hat{J}_z\right) + 2K_yK_z\widehat{\mathrm{Cov}}\left(\hat{J}_y,\hat{J}_z\right) + K_x\mathrm{Cov}\left(\hat{J}_x,\hat{N}\right) + K_y\mathrm{Cov}\left(\hat{J}_y,\hat{N}\right) + K_z\mathrm{Cov}\left(\hat{J}_z,\hat{N}\right) \tag{22}$$

and the phase sensitivity for this detection scenario is

$$\Delta\varphi_{sg} = \frac{\sqrt{\Delta^2\hat{n}_4}}{\left|\langle\hat{J}_x\rangle\cos\varphi + \left(\cos\vartheta\,\langle\hat{J}_y\rangle + \sin\vartheta\langle\hat{J}_z\rangle\right)\sin\varphi\right||\sin\vartheta'|}. \tag{23}$$

This phase sensitivity, too, can be optimized and a closed-form solution for both ϑ'_{opt} and φ_{opt} is possible, see reference [25], Appendix F.

4.3. Phase sensitivity optimization for a balanced homodyne detection scheme
Wenow now consider a BHD scheme at the output port 4 (see Fig. 3), the operator modeling this detection scheme being $\hat{X}_{\phi_L} = (e^{-i\phi_L}\hat{a}_4 + e^{i\phi_L}\hat{a}_4^\dagger)/2$ [28, 38] where ϕ_L is the phase of the local oscillator. We find the variance of the above operator,

$$\Delta^2\hat{X}_{\phi_L} = \frac{1}{4} + \frac{1}{2}\left(\langle\hat{n}_4\rangle - |\langle\hat{a}_4\rangle|^2 + \Re\left\{e^{-i2\phi_L}\Delta^2\hat{a}_4\right\}\right), \tag{24}$$

and the phase sensitivity in this case is

$$\Delta\varphi_{hom} = \frac{\sqrt{\Delta^2\hat{X}_{\phi_L}}}{\left|\sin\frac{\vartheta}{2}\Re\left\{e^{-i(\phi_L+\varphi)}i\langle\hat{a}_0\rangle\right\} + \cos\frac{\vartheta}{2}\Re\left\{e^{-i(\phi_L+\varphi)}\langle\hat{a}_1\rangle\right\}\right|\sin\frac{\vartheta'}{2}}. \tag{25}$$

For the expression of $\Delta^2\hat{X}_{\phi_L}$ in respect with the input field operators see reference [25].

A closed-form expression for both ϑ'_{opt} and φ_{opt} optimizing the above phase sensitivity is given in reference [25], Appendix G.

5. MZI phase sensitivity optimization examples for some input states

In this section we apply the methods discussed in Sections 3 and 4 in order to optimize the phase sensitivity for an unbalanced MZI fed by some input states and having the detection schemes previously discussed.

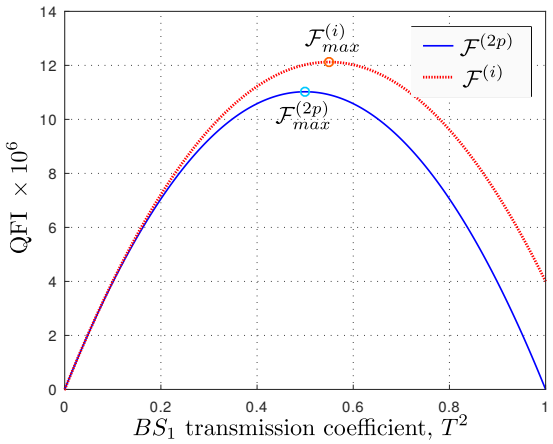

Figure 4. The single- and two-parameter QFI versus the transmission coefficient of BS_1. Parameters used: $|\alpha| = 10^3$, $r = 1.2$, $2\theta_\alpha - \theta = 0$.

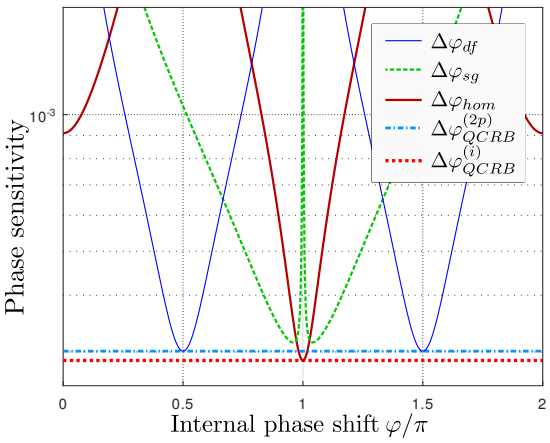

Figure 5. Phase sensitivity for a MZI fed with the input state (26) and with the three considered detection schemes.. Parameters used: $|\alpha| = 10^3$, $r = 1.2$, $2\theta_\alpha - \theta = 0$.

5.1. Coherent plus squeezed vacuum input
The paradigmatic non-classical input state showing both a theoretical and a practical interest is the coherent plus squeezed vacuum input [4, 17, 39, 40],

$$|\psi_{in}\rangle = |\alpha_1\xi_0\rangle, \tag{26}$$

where the coherent state in port 1 is a vacuum state $|0\rangle$ displaced by Glauber operator $\hat{D}_1(\alpha) = e^{\alpha\hat{a}_1^\dagger - \alpha^*\hat{a}_1}$ [35] and we denote $\alpha = |\alpha|e^{i\theta_\alpha}$. The squeezed vacuum in port 0 is the

result of applying the squeezing operator $\hat{S}_0(\xi) = e^{1/2\left(\xi^* \hat{a}_0^2 - \xi(\hat{a}_0^\dagger)^2\right)}$ [35, 41, 42], where $\xi = re^{i\theta}$, $r \in \mathbb{R}^+$ denotes the squeezing factor and θ is the phase of the squeezed state.

The dependence of both the single- and two-parameter QFI in respect with the BS_1 transmission coefficient is depicted in Fig. 4. While, as expected from Section 3.1, for the two-parameter QFI the optimum is found in the balanced case yielding $\mathcal{F}_{max}^{(2p)} = |\alpha|^2 e^{2r} + \sinh^2 r$ [17], for the single-parameter QFI this is no longer true. Indeed, we find $T_{opt} \approx \sqrt{0.54} \approx 0.74$ and a maximum QFI $\mathcal{F}_{max}^{(i)} = 12.1 \times 10^6$, to be compared with the two-parameter QFI optimum value $\mathcal{F}_{max}^{(2p)} = 11 \times 10^6$.

The phase sensitivity for a MZI fed by the input state (26) is depicted in Fig. 5. The optimum performance for both the single- and difference-intensity detection schemes is found when BS_2 is balanced, too [25]. For these detection schemes the QCRB is given by equation (10). As depicted in Fig. 5, while the single-mode detection scheme (thick light-green dashed curve) is sub-optimal, the difference intensity scheme (solid thick blue curve) is nearly optimal.

The BHD scheme on the other hand, having access to an external phase reference, is able to go beyond the two-parameter QCRB (light-blue dash-dotted horizontal line). By optimizing BS_2 we obtain $T' = 0.67$ and, as seen from Fig. 5, the BHD (dark-red solid curve) goes beyond the two-parameter QCRB and approaches the single-parameter QFI-induced limit (12) (thick dotted red horizontal line).

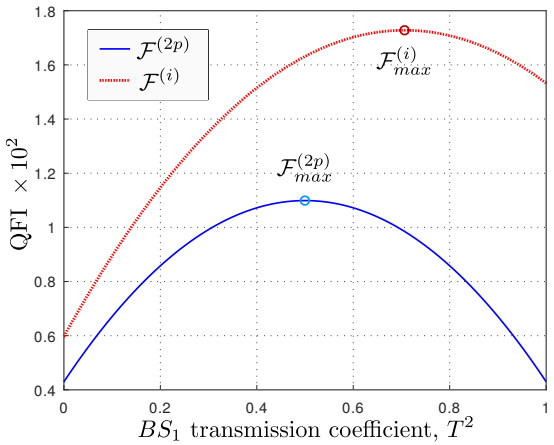

Figure 6. The single- and two-parameter QFI versus the transmission coefficient of BS_1 for the input state (27). Parameters used: $|\alpha| = 3$, $r = 1.2$, $z = 0.7$, PMC from equation (28).

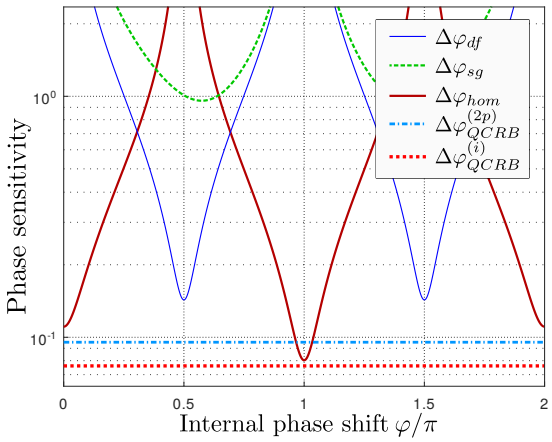

Figure 7. Phase sensitivity of a MZI fed by the input state (27) and with the three considered detection schemes. Parameters used: $|\alpha| = 3$, $r = 1.2$, $z = 0.7$, PMC from equation (28).

5.2. Squeezed-coherent plus squeezed vacuum input

Consider now the squeezed-coherent plus squeezed vacuum input state [14, 22, 24],

$$|\psi_{in}\rangle = |(\alpha\zeta)_1 \xi_0\rangle = \hat{D}_1(\alpha)\, \hat{S}_1(\zeta)\, \hat{S}_0(\xi)\, |0\rangle \tag{27}$$

where the squeezer in input port 1 is characterized by $\zeta = ze^{i\phi}$. All QFIs are maximized if we impose the input PMC [22, 38],

$$\begin{cases} 2\theta_\alpha - \theta = 0 \\ 2\theta_\alpha - \phi = \pm\pi. \end{cases} \tag{28}$$

When no external phase reference is available, the optimum two-parameter QFI is found in the balanced case yielding $\mathcal{F}^{(2p)}_{max} = |\alpha|^2 e^{2r} + \sinh^2(r+z)$ [22, 38]. For single- and difference-intensity detection schemes the optimum phase sensitivity is also found for a balanced MZI [22, 23]. This is no longer true for the BHD scheme. Indeed, the relevant QFI is single-parameter one and the optimum transmission coefficient is found following the method described in Section 3.2.

As an application for the input state (27) we consider a low-coherent scenario ($|\alpha|^2 \sim \sinh^2 r$), relevant *e. g.* for quantum-enhanced biological sensing [8, 9]. In Fig. 6 we depict the dependence on both single- and two-parameter QFI in respect with the transmission coefficient of BS_1. As expected, the two-parameter QFI is optimized in the balanced case, while the optimum transmission coefficient that maximizes the single-parameter QFI is found to be $T_{opt} \approx \sqrt{0.705} \approx 0.84$.

The phase sensitivity for a MZI fed by the input state (27) is given in Fig. 7. Both the single-intensity and difference-intensity detection schemes yield sub-optimal results in respect with the two-parameter QCRB (light blue dash-dotted horizontal line). By optimizing the second BS for the BHD scheme we get the value $T'_{opt} = 0.46$. The BHD scheme, as seen from Fig. 7 (solid dark red curve), goes beyond this two-parameter QCRB and although slightly sub-optimal, it approaches the single-parameter QFI induced QCRB (red thick dotted horizontal line).

6. Conclusions

In this paper we addressed the phase sensitivity optimization for an unbalanced Mach-Zehnder interferometer. Guided by the quantum Fisher information, we were able to unambiguously optimize the transmission coefficient of the first beam splitter.

Since the phase sensitivity is detection scheme dependent, we had to take this aspect into consideration when optimizing the second beam splitter. The problem turned out to be a two-variable optimization problem, the optimum phase sensitivity depending on both the transmission coefficient of the second beam splitter and the total internal phase shift of the interferometer.

We provided examples both in the high- and low-intensity regimes, where the phase sensitivity for three often used detection schemes was evaluated. For the discussed scenarios we showed that when an external phase reference is available, it turns out that the best performance in terms of phase sensitivity arises for a non-balanced Mach-Zehnder interferometer.

7. Acknowledgments

It is acknowledged that this research was supported from the Nucleu Project, PN 19 06 01 05. It is also acknowledged that this work has been supported by the Extreme Light Infrastructure Nuclear Physics (ELI-NP) Phase II, a project co-financed by the Romanian Government and the European Union through the European Regional Development Fund and the Competitiveness Operational Programme (1/07.07.2016, COP, ID 1334).

Appendix A. The C-coefficients for the two-parameter QFI

The C-coefficients from Section 3.1 are defined by

$$\begin{cases} C_0 = 4\left(\Delta^2\hat{J}_z - \frac{\left(\mathrm{Cov}\left(\hat{J}_z,\hat{N}\right)\right)^2}{\Delta^2\hat{N}}\right) \\ C_1 = 16\left(\Delta^2\hat{J}_y - \Delta^2\hat{J}_z - \frac{\left(\mathrm{Cov}\left(\hat{J}_y,\hat{N}\right)\right)^2}{\Delta^2\hat{N}} + \frac{\left(\mathrm{Cov}\left(\hat{J}_z,\hat{N}\right)\right)^2}{\Delta^2\hat{N}}\right) \\ C_2 = -16\left(\widehat{\mathrm{Cov}}\left(\hat{J}_y,\hat{J}_z\right) - \frac{\mathrm{Cov}\left(\hat{J}_y,\hat{N}\right)\mathrm{Cov}\left(\hat{J}_z,\hat{N}\right)}{\Delta^2\hat{N}}\right) \end{cases} \tag{A.1}$$

Appendix B. The C'-coefficients for the single-parameter QFI

The C'-coefficients used in equation (13) are given by: $C'_0 = 4\Delta^2\hat{J}_z$, $C'_1 = 16\left(\Delta^2\hat{J}_y - \Delta^2\hat{J}_z\right)$, $C'_2 = -16\widehat{\mathrm{Cov}}\left(\hat{J}_y, \hat{J}_z\right)$, $C'_3 = -4\mathrm{Cov}\left(\hat{J}_z, \hat{N}\right)$ and $C'_4 = 8\mathrm{Cov}\left(\hat{J}_y, \hat{N}\right)$.

References

[1] The LIGO Scientific Collaboration 2013 *Nat. Photonics* **7** 613–619
[2] Acernese F *et al.* 2014 *Class. Quantum Grav.* **32** 024001
[3] Tse M *et al.* 2019 *Phys. Rev. Lett.* **123** 231107
[4] Caves C M 1981 *Phys. Rev. D* **23** 1693–1708
[5] Giovannetti V, Lloyd S and Maccone L 2006 *Phys. Rev. Lett.* **96**(1) 010401
[6] Acín A *et al.* 2018 *New J. Phys.* **20** 080201
[7] Backes K M *et al.* 2021 *Nature* **590** 238
[8] Taylor M A *et al.* 2013 *Nature Photonics* **7** 229
[9] Taylor M A and Bowen W P 2016 *Physics Reports* **615** 1–59
[10] Helstrom C 1967 *Physics Letters A* **25** 101–102
[11] Helstrom C 1968 *IEEE Trans. Inf. Theory* **14** 234–242
[12] Braunstein S L and Caves C M 1994 *Phys. Rev. Lett.* **72** 3439–3443
[13] Paris M G A 2009 *Int. J. Quantum Inf.* **07** 125–137
[14] Paris M G 1995 *Phys. Lett. A* **201** 1328
[15] Pezzé L and Smerzi A 2006 *Phys. Rev. A* **73** 011801(R)
[16] Pezzé L, Smerzi A, Khoury G, Hodelin J F and Bouwmeester D 2007 *Phys. Rev. Lett.* **99** 223602
[17] Pezzé L and Smerzi A 2008 *Phys. Rev. Lett.* **100** 073601
[18] Lang M D and Caves C M 2013 *Phys. Rev. Lett.* **111** 173601
[19] Sparaciari C, Olivares S and Paris M G A 2016 *Phys. Rev. A* **93** 023810
[20] Ataman S, Preda A and Ionicioiu R 2018 *Phys. Rev. A* **98** 043856
[21] Jarzyna M and Demkowicz-Dobrzański R 2012 *Phys. Rev. A* **85** 011801(R)
[22] Ataman S 2020 *Phys. Rev. A* **102** 013704
[23] Ataman S 2022 *Phys. Rev. A* **105** 012604
[24] Preda A and Ataman S 2019 *Phys. Rev. A* **99** 053810
[25] Mishra K K and Ataman S 2022 *Phys. Rev. A* **106** 023716
[26] Zhong W, Xu P and Sheng Y 2020 *Sci. China Phys. Mech. Astron.* **63** 260312
[27] Yuen H P and Chan V W S 1983 *Opt. Lett.* **8** 177–179
[28] Gard B T *et al.* 2017 *EPJ Quantum Technology* **4** 4
[29] Birrittella R J, Alsing P M and Gerry C C 2021 *AVS Quantum Science* **3** 014701
[30] Zhong W, Huang Y, Wang X and Zhu S L 2017 *Phys. Rev. A* **95** 052304
[31] Zhong W, Zhou L and Sheng Y B 2021 *Phys. Rev. A* **103** 042611
[32] Wu J Y, Toda N and Hofmann H F 2019 *Phys. Rev. A* **100** 013814
[33] Shukla G, Salykina D, Frascella G, Mishra D K, Chekhova M V and Khalili F Y 2021 *Opt. Express* **29** 95–104
[34] Wang S and Zhang J D 2023 *Optics Communications* **527** 128987
[35] Gerry C and Knight P 2005 *Introductory Quantum Optics* (Cambridge University Press)
[36] Yurke B, McCall S L and Klauder J R 1986 *Phys. Rev. A* **33** 4033
[37] Campos R A, Saleh B E A and Teich M C 1989 *Phys. Rev. A* **40** 1371–1384
[38] Ataman S 2019 *Phys. Rev. A* **100** 063821
[39] Xiao M, Wu L A and Kimble H J 1987 *Phys. Rev. Lett.* **59** 278–281
[40] Schnabel R 2017 *Physics Reports* **684** 1 – 51
[41] Yuen H P 1976 *Phys. Rev. A* **13** 2226–2243
[42] Stoler D 1970 *Phys. Rev. D* **1** 3217–3219